

Supporting information

Water-soluble pyridine based colorimetric chemosensor for naked eye detection of silver ion: Design, synthesis, spectral and theoretical investigation

B. Annaraj and M.A. Neelakantan*

*Chemistry Research Centre, National Engineering College, K.R.Nagar, Kovilpatti - 628 503,
Thoothukudi District, Tamil Nadu, India*

Email: maneels@rediffmail.com; drmaneelakantan@gmail.com

Theoretical calculation:

To examine the mode of interaction and to understand the sensing behavior of **L** with Ag^+ , we carried out density functional theory (DFT) calculations with Becke's three parametrized Lee-Yang-Parr (B3LYP) [1] exchange functional with 6-31G* basis sets, using a suite of Gaussian 09 programs [2]. Molecular geometry of the sensor (**L**) was optimized by 6-31G* level. The optimized structure of **L** was very close to the single crystal X-ray diffraction structure. The structure of **L** – Ag^+ was calculated by B3LYP/6-31g(d,p) + Lanl2DZ effective core potential (ECP). The electronic absorption spectra of **L** and **L**+ Ag^+ have been calculated using TD-DFT calculation.

The optimized geometries of **L** and its 1:1 complex with Ag^+ ion are shown in the figure, which displays the effective binding sites, namely azoethine-N, Phenolic-OH and aliphatic-OH for Ag^+ ion (Fig. S12). The pyridine moiety of **L** has a HOMO character predominantly, whereas LUMO orbital covers whole the molecule (Fig. S13). In the presence of Ag^+ , the HOMO and LUMO orbitals are located on **L** and Ag^+ by well separated manner. This type of HOMO-LUMO distribution is clearly indicating the significant electron transfer from one part of **L** to another i.e metal centre to ligand. The energy difference between HOMO-LUMO of **L** is 4.39 eV and the binding of Ag^+ ions with **L** reduces the energy gap to 1.71 eV. It implies that addition of the metal ions leads to the stabilization of the HOMO and LUMO of the fluorophores. The DFT calculations were carried out to study the interaction between **L** and Pb^+ ions. The frontier molecular orbital of **L**+ Pb (Fig. S14) is completely different from that of **L**+ Ag^+ clearly demonstrates the non interaction between **L** and Pb^+ . The computed UV-Visible spectra of **L** and **L**+ Ag (Fig. S15) are comparable with that of the experimental result.

1. P.J. Stephens, F.J. Devlin, C.F. Chabalowski, M.J. Frisch, *J. Phys. Chem.* 1994, **98** 11623–11627.
2. M.J. Frisch, G.W. Trucks, H.B. Schlegel, G.E. Scuseria, M.A. Robb, J.R. Cheeseman, J.A. Montgomery, T.J. Vreven, K.N. Kudin, J.C. Burant, J.M. Millam, S.S. Iyengar, J.Tomasi, V. Barone, B. Mennucci, M. Cossi, G. Scalmani, N. Rega, G.A. Petersson, H. Nakatsuji, M. Hada, M. Ehara, K. Toyota, R. Fukuda, J. Hasegawa, M. Ishida, T. Nakajima, Y. Honda, O. Kitao, H. Nakai, M. Klene, X. Li, J.E. Knox, H.P. Hratchian, J.B. Cross, C.

Adamo, J. Jaramillo, R. Gomperts, R.E. Stratmann, O. Yazyev, A.J.Austin, R. Cammi, C. Pomelli, J.W. Ochterski, P.Y. Ayala, K. Morokuma, G.A. Voth, P. Salvador, J.J. Dannenberg, V.G. Zakrzewski, S. Dapprich, A.D. Daniels, M.C. Strain, O. Farkas, D.K. Malick, A.D. Rabuck, K. Raghavachari, J.B. Foresman, J.V. Ortiz, Q. Cui, A.G. Baboul, S. Clifford, J. Cioslowski, B.B. Stefanov, G. Liu, A. Liashenko, P. Piskorz, I. Komaromi, R.L. Martin, D.J. Fox, T. Keith, M.A. Al-Laham, C.Y. Peng, A. Nanayakkara, M. Challacombe, P.M.W. Gill, B. Johnson, W. Chen, M.W. Wong, C. Gonzalez, J.A. Pople, Gaussian 03, Revision E. 01, Gaussian, Inc., Wallingford, CT, 2004.

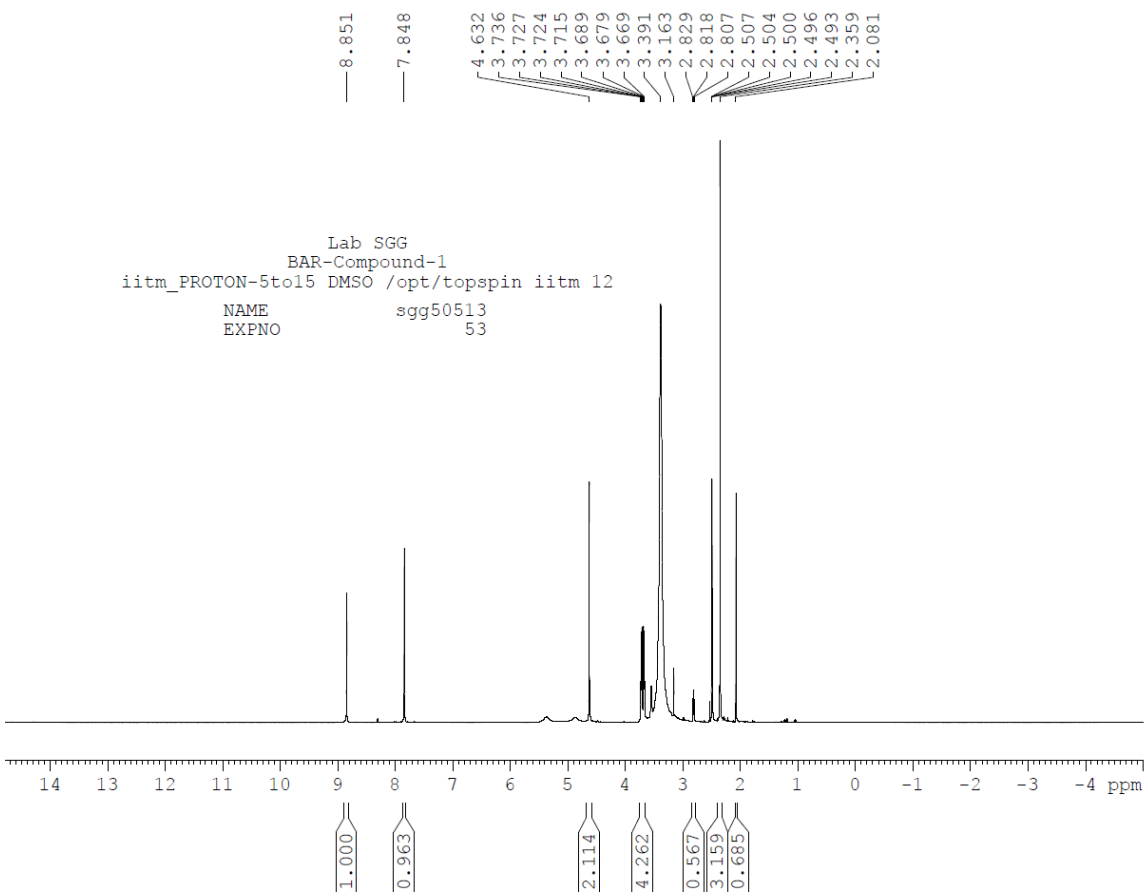


Fig. S1 ^1H NMR Spectrum of **L**

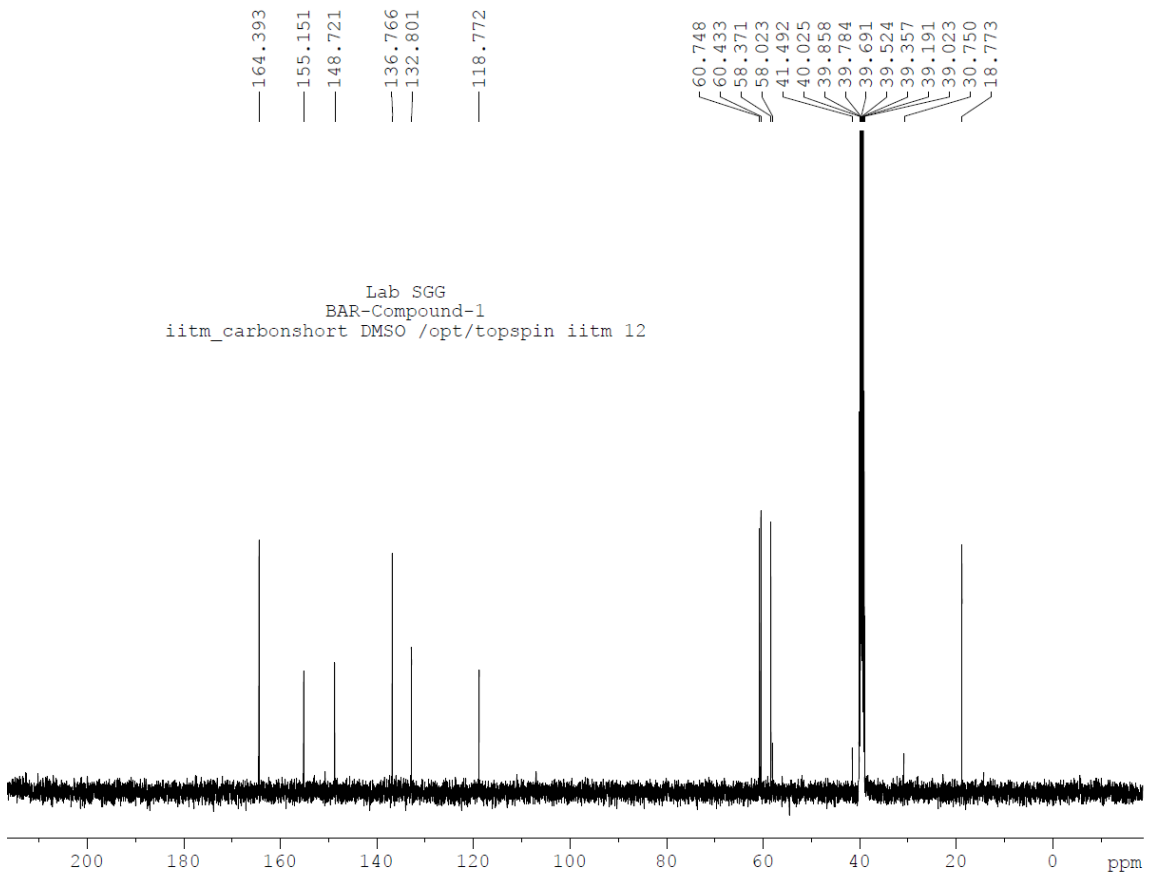


Fig. S2 ^{13}C NMR Spectrum of **L**

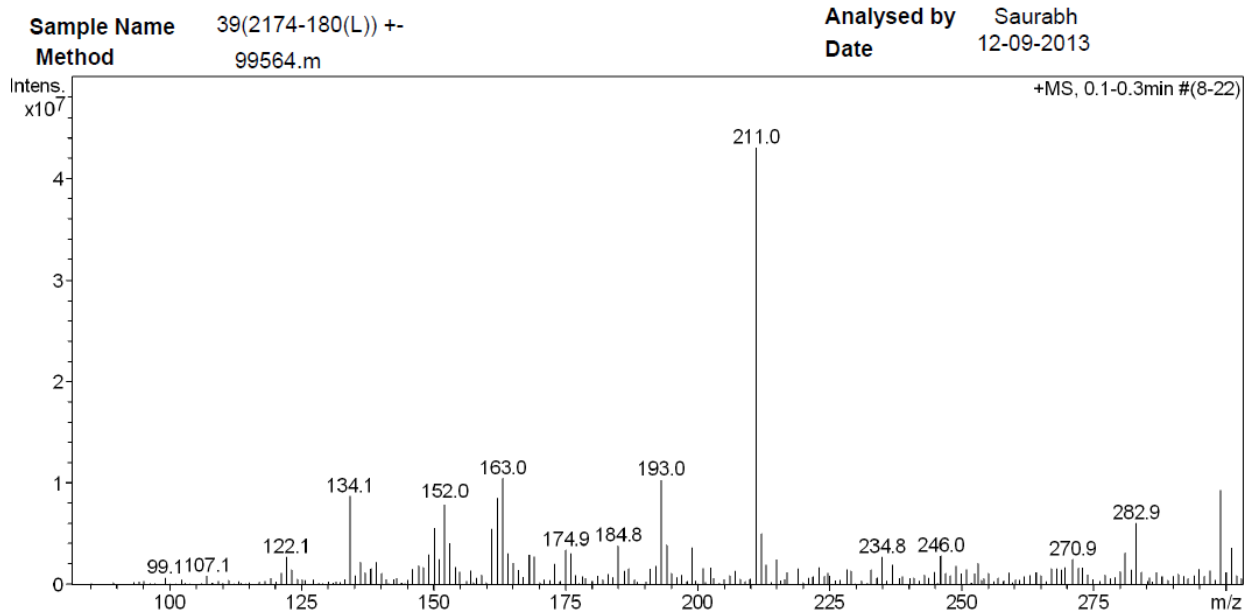


Fig. S3 ESI Mass of L

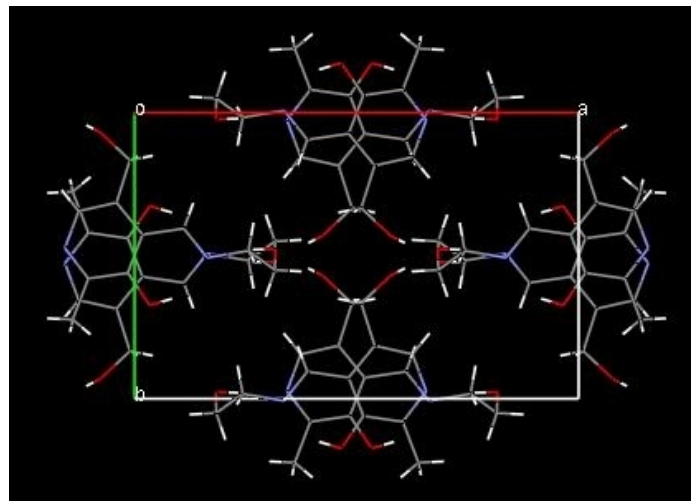


Fig. S4 Crystal packing diagram of L viewed along C axis

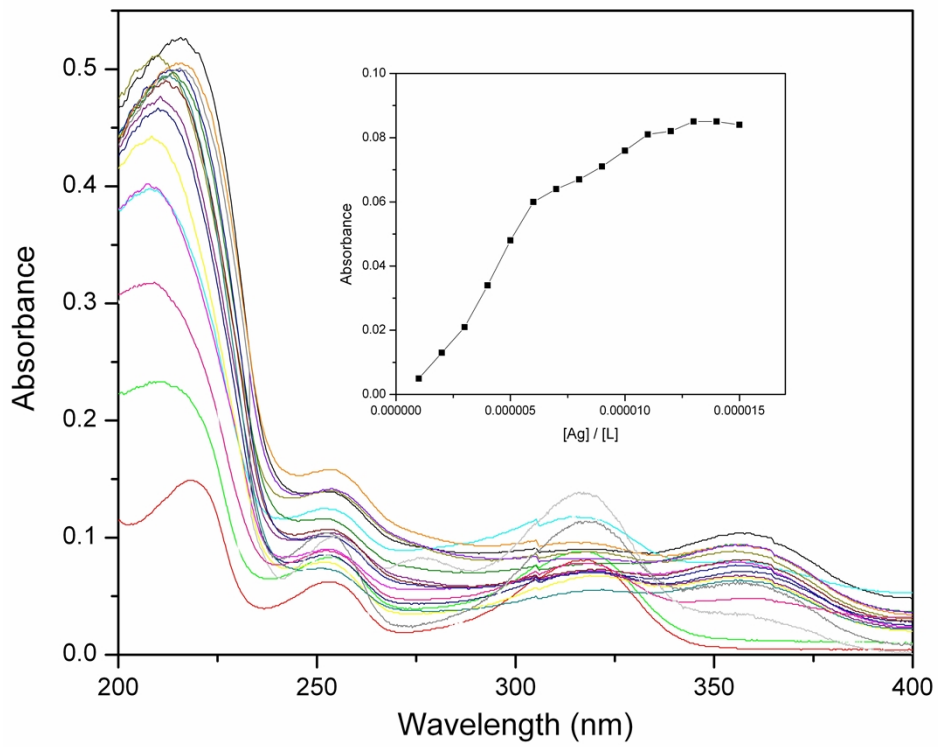


Fig. S5 Electronic absorption spectra of **L** (20 μM) in presence of different equivalents (0.5-15) of Ag^+ ions

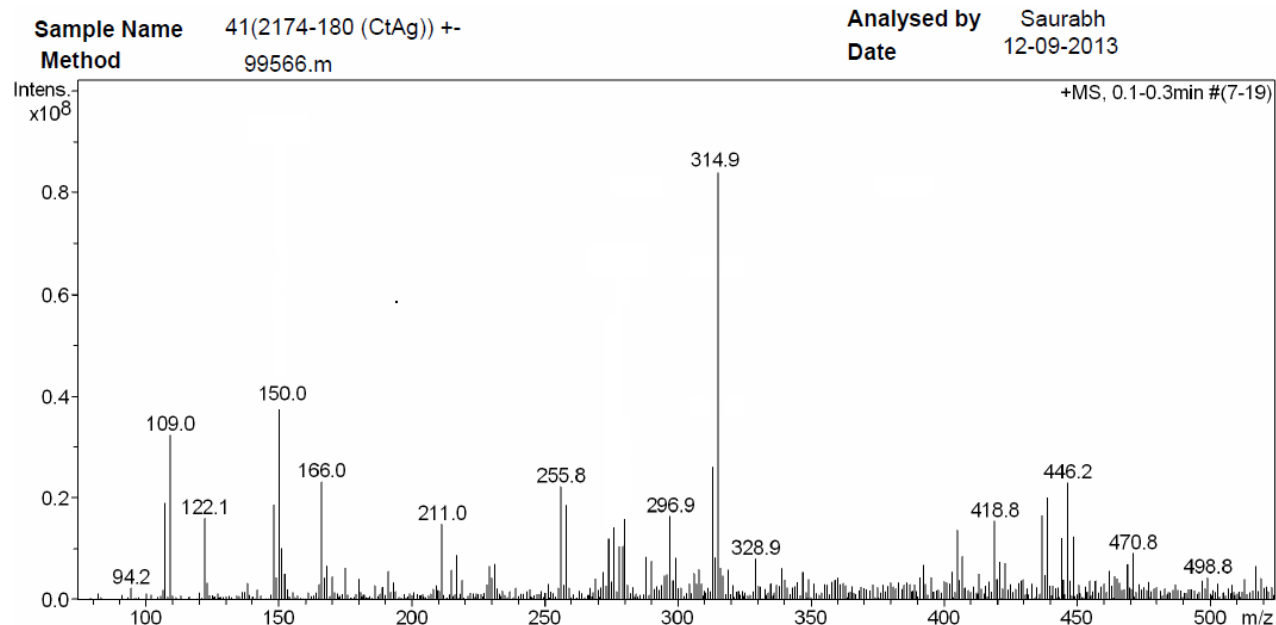


Fig. S6 ESI Mass spectrum of L+Ag

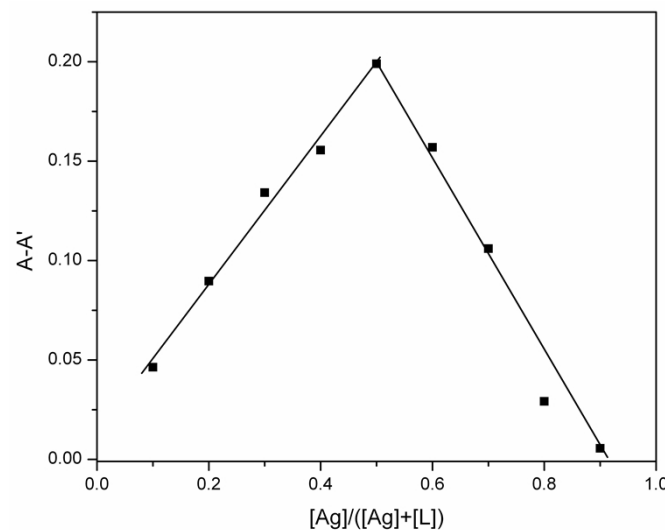


Fig. S7 JOB Plot for L and Ag showing the 1:1 complex formation

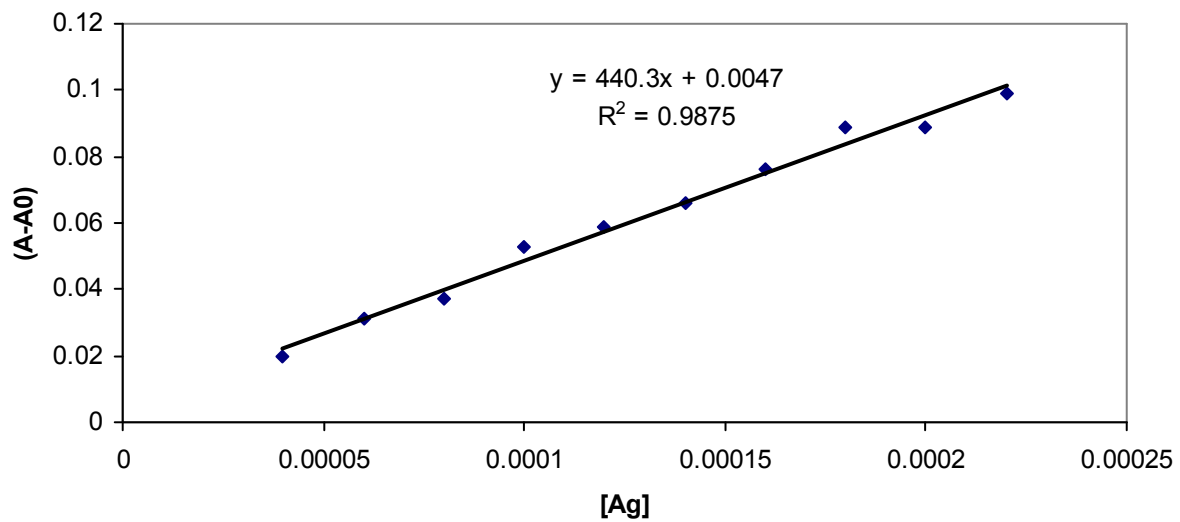


Fig. S8 Plot for the Calculation of detection limit of **L** (20 μM) towards Ag ion

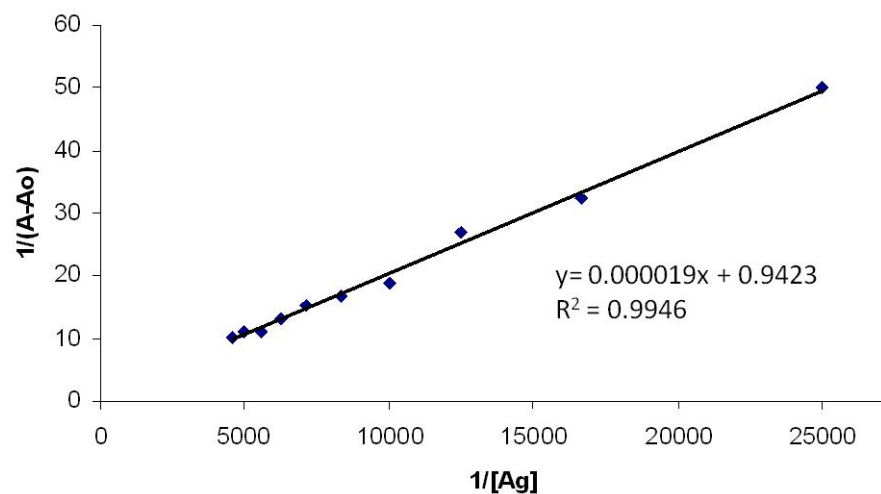


Fig. S9 Benesi-Hilderbrand Plot for the binding of Ag ion with **L**

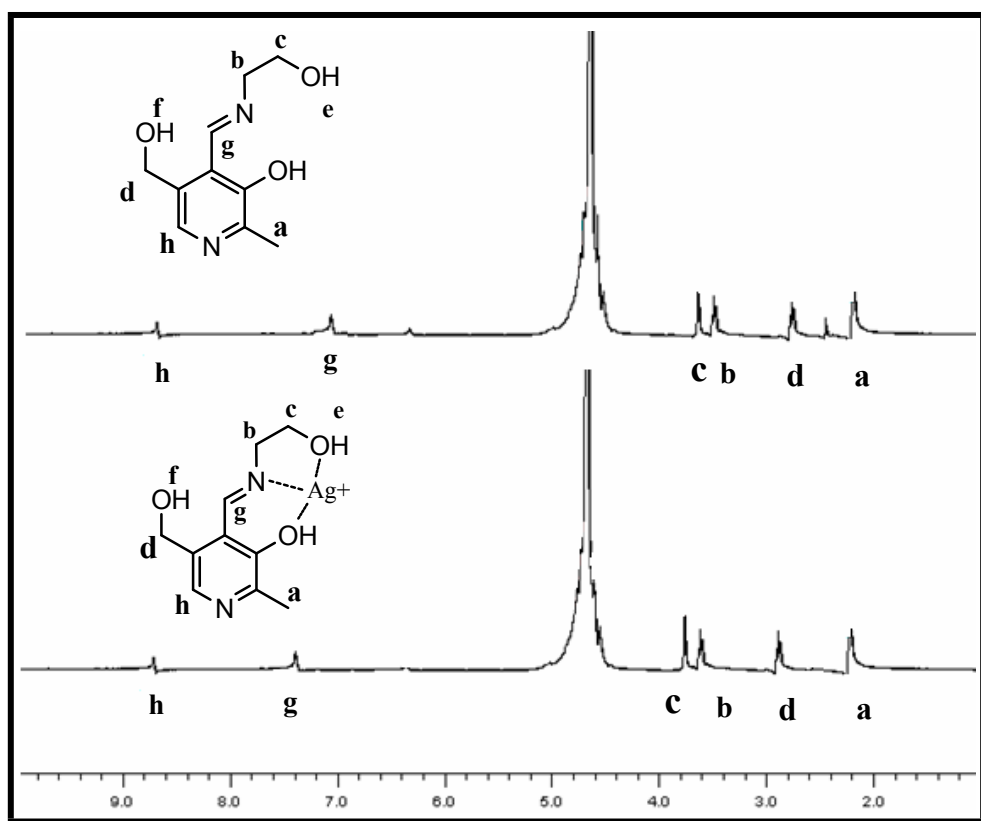


Fig. S10 ^1H -NMR Spectra of **L** and **L+Ag** recorded in D_2O

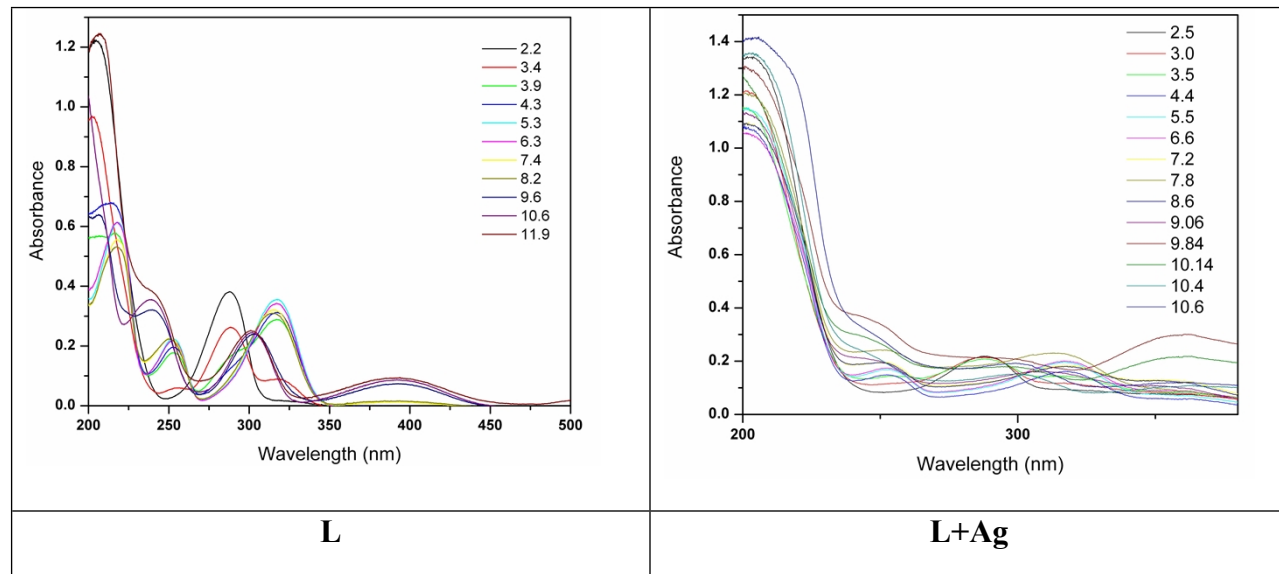


Fig. S11 Effect of pH on the UV-Visible absorption of **L** and **L+Ag**

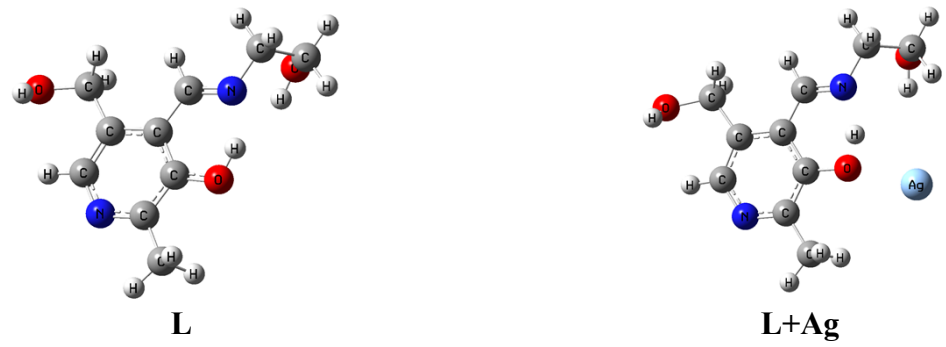


Fig. S12 Optimized geometry of **L** and **L+Ag**

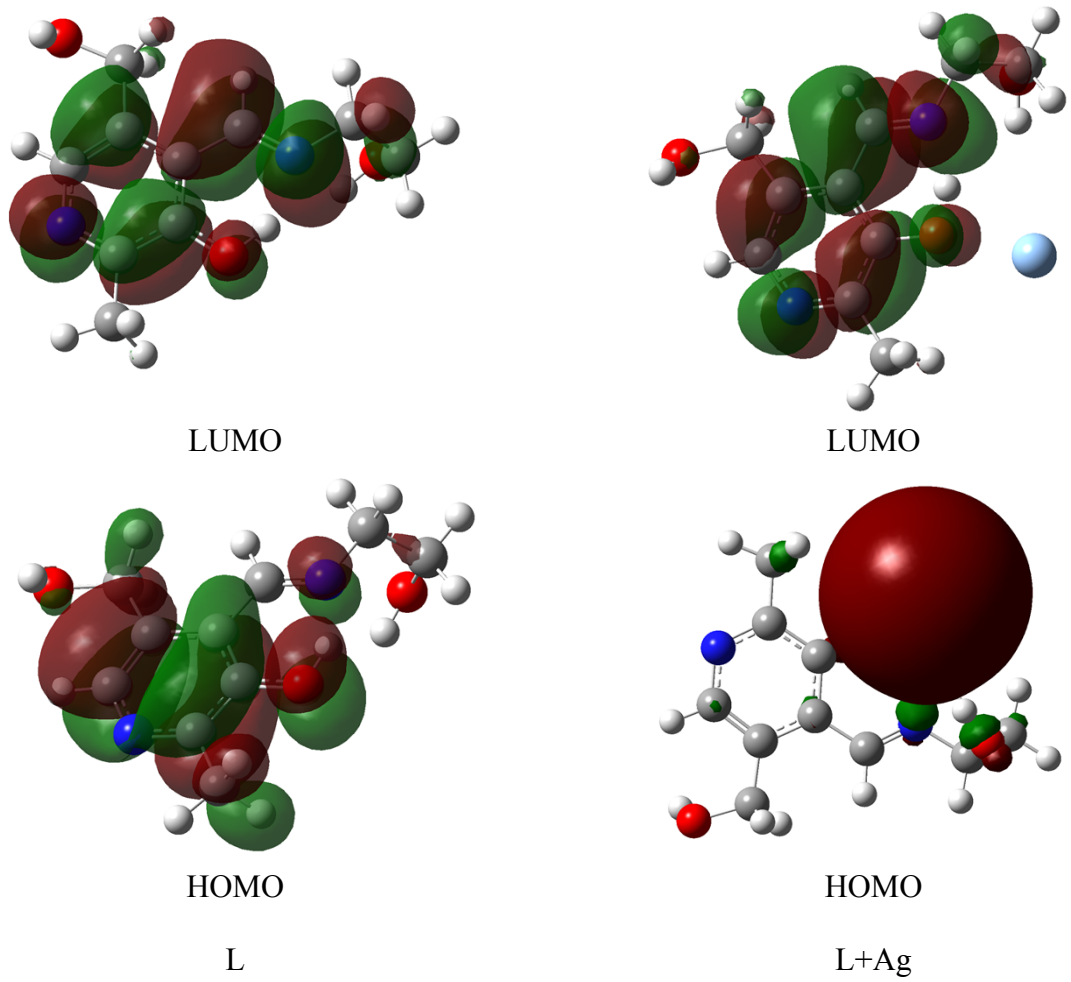
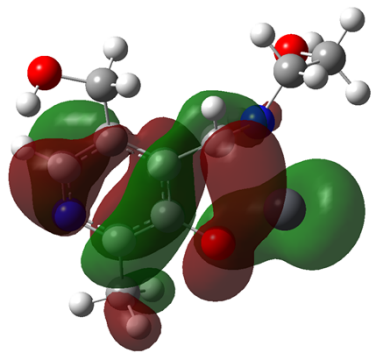
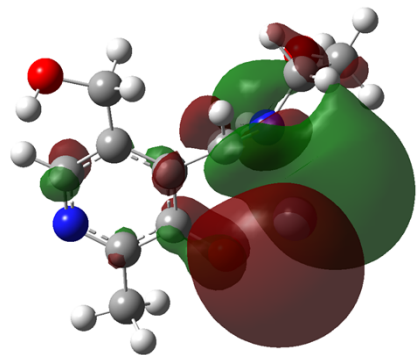


Fig. S13 Frontier molecular orbitals of **L** and **L+Ag**



HOMO (Pb)



LUMO (Pb)

Fig. S14 Frontier molecular orbitals of **L** and **L+Pb**

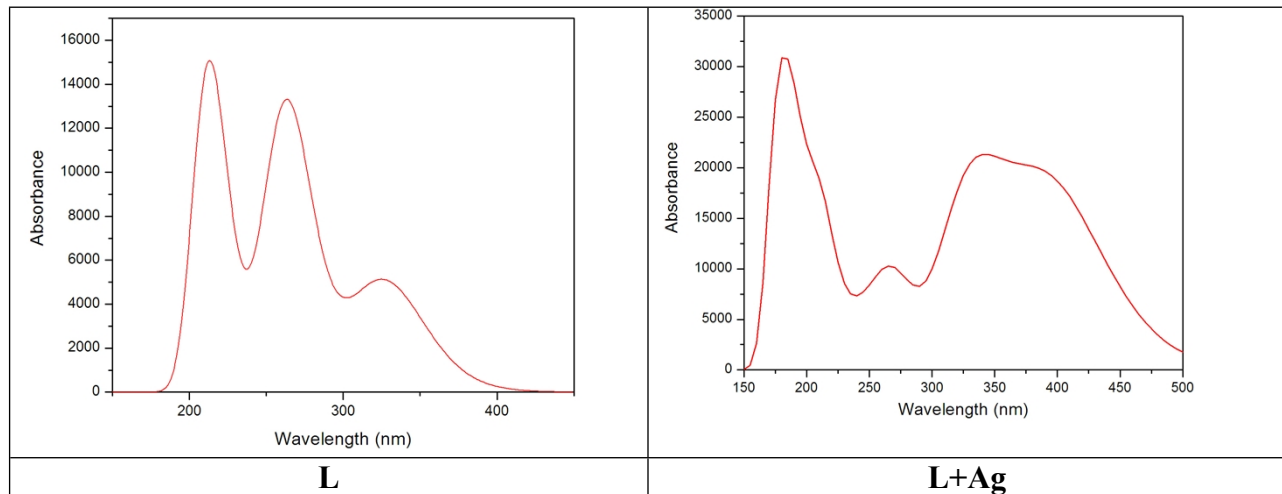


Fig. S15 Computed UV-Visible spectra of **L** and **L+Ag**

Table S1 Crystal Data of **L**

Parameters	L
Empirical formula	C10 H14 N2 O3
Formula weight	210.23
Temperature	296(2) K
Wavelength	0.71073 Å
Crystal system, space group	Monoclinic, C2/c
Unit cell dimensions	a = 16.3383(13) Å alpha = 90 deg. b = 9.6603(13) Å beta = 113.262(7) deg.
	c = 13.6431(12) Å gamma = 90 deg.
Volume	1978.3(4) Å^3
Z, Calculated density	8, 1.412 Mg/m^3
Absorption coefficient	0.105 mm^-1
F(000)	896
Crystal size	0.40 x 0.35 x 0.30 mm
Theta range for data collection	2.51 to 28.29 deg.
Limiting indices	-21<=h<=21, -12<=k<=12, -18<=l<=14
Reflections collected / unique	7654 / 2411 [R(int) = 0.0257]
Completeness to theta = 28.29	97.90%
Absorption correction	Semi-empirical from equivalents
Max. and min. transmission	0.9691 and 0.9591
Refinement method	Full-matrix least-squares on F^2
Data / restraints / parameters	2411 / 0 / 146
Goodness-of-fit on F^2	0.879
Final R indices [I>2sigma(I)]	R1 = 0.0432, wR2 = 0.1242
R indices (all data)	R1 = 0.0605, wR2 = 0.1483
Largest diff. peak and hole	0.234 and -0.276 e.Å^-3

Table S2 Selected bond length and bond angles of **L**

Bond Length (Å)	
O(1)-C(5)	1.3368(18)
O(1)-H(1O1)	0.82
N(1)-C(8)	1.2679(19)
N(1)-C(9)	1.4534(19)
O(3)-C(10)	1.414(2)
O(3)-H(3O3)	0.89(3)
O(2)-C(1)	1.404(2)
O(2)-H(2O2)	0.92(3)
C(1)-C(2)	1.511(2)
C(1)-H(1A)	0.97
C(1)-H(1B)	0.97
C(2)-C(3)	1.371(2)
C(2)-C(6)	1.407(2)
C(6)-C(5)	1.399(2)
C(6)-C(8)	1.459(2)
C(8)-H(9)	0.93
C(9)-C(10)	1.515(2)
C(5)-C(4)	1.407(2)
C(4)-N(2)	1.321(2)
C(4)-C(7)	1.492(2)
N(2)-C(3)	1.346(2)
C(3)-H(4)	0.93
Bond Angle (°)	
C(5)-O(1)-H(1O1)	109.5
C(8)-N(1)-C(9)	119.85(14)
C(10)-O(3)-H(3O3)	114.2(15)
C(1)-O(2)-H(2O2)	111.1(15)
O(2)-C(1)-C(2)	113.04(14)
C(3)-C(2)-C(6)	117.73(14)
C(3)-C(2)-C(1)	120.89(14)
C(6)-C(2)-C(1)	121.36(13)
C(5)-C(6)-C(2)	118.07(13)
C(5)-C(6)-C(8)	119.93(13)
C(2)-C(6)-C(8)	121.98(13)
N(1)-C(8)-C(6)	121.03(14)
N(1)-C(8)-H(9)	119.5
C(6)-C(8)-H(9)	119.5
N(1)-C(9)-C(10)	110.29(13)
O(1)-C(5)-C(6)	122.74(13)

O(1)-C(5)-C(4)	117.48(13)
C(6)-C(5)-C(4)	119.78(13)
N(2)-C(4)-C(5)	121.05(14)
N(2)-C(4)-C(7)	119.11(14)
C(5)-C(4)-C(7)	119.84(14)
C(4)-N(2)-C(3)	119.19(13)
N(2)-C(3)-C(2)	124.13(14)
N(2)-C(3)-H(4)	117.9
C(2)-C(3)-H(4)	117.9

Table S3 Analytical results for the detection of silver ions in real samples

Sample	Determined [Ag ⁺] (μM) ^a	Added [Ag ⁺] (μM)	By Test kit [Ag ⁺] (μM)	By Absorption spectra [Ag ⁺] (μM)
Drinking water	0.02	40	38-40	39.08 ± 0.3
Bore well water	0.08	40	38-41	40.20 ± 0.8
Tap water	0.05	40	39-41	39.80 ± 0.5

^a Analysis by AAS